Effects of nonzero bandwidth on direction of arrival estimators in array signal processing

J. Sorelius
R.L. Moses
T. Söderström
A.L. Swindlehurst

Indexing terms: Array signal processing, DOA estimation

Abstract: The authors consider the impact of a small but nonzero bandwidth on narrowband direction-of-arrival (DOA) estimation using an array of sensors. They derive expressions for the DOA error for three commonly used array processing algorithms: MUSIC, ESPRIT and weighted subspace fitting (WSF). The error expressions are found by a perturbation analysis of these algorithms for small relative bandwidths of the sources. The perturbation-based error predictions are compared to the exact deviation for some special cases of interest.

1 Introduction

In this paper we consider the effect of bandwidth on direction-of-arrival (DOA) estimates. Our problem is motivated by communications and sensor problems in which the bandwidths of the source signals, while small, may not be negligibly small, such as, for example, in radar, acoustics and underwater array processing. Our interest is to quantify the error (and variance) that results from using narrowband DOA estimators when the sources have nonzero bandwidths.

An important and popular class of narrowband DOA estimation algorithms is based on decomposing the array covariance matrix into a low-rank signal subspace and an orthogonal noise subspace. The low-rank structure arises from a zero-bandwidth assumption; when the signals have a nonzero bandwidth, the low-rank structure of the signal subspace is lost (see [1] for a discussion on the effect of bandwidth on the distribution of the eigenvalues of the covariance matrix). Correspondingly, the statistical properties of the DOA estimates, and in particular the DOA errors, are affected.

One alternative to DOA estimation for sources with nonzero bandwidth is to use wideband source location algorithms (see, for example, [2, 3] and their references). However, these algorithms are more complex than their narrowband counterparts, so the use of narrowband algorithms is preferred when the bandwidths are small enough that the DOA error is neglible or tolerable.

In this work we quantify the error in the DOA estimates for three popular subspace-based narrowband DOA estimators: MUSIC, ESPRIT and weighted subspace fitting (WSF). Specifically, we assume multiple signals of nonzero bandwidth impinging on an array of sensors and give analytical expressions for the resulting error in the estimates of the directions of arrival.

The analysis is based on a series expansion of the signal and noise subspaces of the array covariance matrix as a function of the relative bandwidths of the source signals; as such, the analysis applies to cases where the relative bandwidths are 'small'. We compare our expressions to the true deviation resulting from sources with nonzero bandwidth for some cases of interest.

Our error analysis is a perturbation analysis of the array covariance matrix, and is similar in principle to several related perturbation analyses on, for example, sensor positioning errors and uncertainties in the sensor gains and phases. First-order DOA variance due to finite-sample effects and to sensor errors are studied, for example, in [4–10] and their references. DOA bias has been analysed in [11–13] using second-order techniques. The above references assume a perturbation that retains the low-rank structure of the signal subspace. In contrast, the nonzero bandwidth of the source signals destroys this low-rank property. In [14, 15] a general array perturbation analysis is presented, in which a low-rank signal subspace is not assumed. In related earlier work [16], which was in part based on [14, 15], we studied the effect of multipath-induced source angular spread on DOA estimation, another problem in which the low-rank subspace structure is lost. Following [16], it is straightforward to include the effect of a finite sample length (i.e. variance) in the error analysis. Since this extension is straightforward, we only consider it briefly in this paper, and focus on obtaining the expressions for the error resulting from the nonzero bandwidth.

2 Model and assumptions

In the following Section we define the (complex-valued) signal model used throughout the paper, and give a derivation of the array output covariance matrix. The

IEE Proceedings online no. 19982428

Paper first received 8th December 1997 and in revised from 27th May 1998

J. Sorelius and T. Söderström are with the Systems and Control Group, Uppsala University, PO Box 27, SE-751 03 Uppsala, Sweden

R.L. Moses is with the Department of Electrical Engineering, The Ohio State University, 2015 Neil Avenue, Columbus, OH 43210, USA

A.L. Swindlehurst is with the Department of Electrical and Computer Engineering, Brigham Young University, 459 CB, Provo, UT 84602, USA

signals received at the array $\{y_k(t)\}_{k=1}^n$ are, of course, real-valued. Let $y_k(t)$ be defined as

$$y_k(t) = \alpha_k(t)\cos(\omega_k t + \varphi_k(t)) \tag{1}$$

It is clear that $y_k(t)$ can also be written as

$$y_k(t) = \mathrm{Re}\left\{\alpha_k(t)e^{i\varphi_k(t)}e^{i\omega_k t}\right\} = \mathrm{Re}\left\{d_k(t)e^{i\omega_k t}\right\} \tag{2}$$

where $d_k(t) \triangleq \alpha_k(t)e^{i\varphi_k(t)}$ is the complex envelope of $y_k(t)$ [17]. It is mathematically convenient (see, for example, [17]) to work with complex signals, and this is the approach that is taken in this paper. It should, however, be clear that to each complex modulated signal $s_k(t) \triangleq d_k(t)e^{i\omega_k(t)}$ corresponds a real-valued received signal $y_k(t)$ as described by eqn. 2.

Assume that n (complex modulated) signals $\{s_k(t)\}_{k=1}^n$ impinge on an array of m sensors. The signals are assumed to be uncorrelated stationary stochastic processes. Each signal arrives from an angle θ_k and has a symmetric spectral density $S_k(\omega)$, centred around the carrier frequency ω_k. Its total power is defined by

$$q_k \triangleq \frac{1}{2\pi}\int_{-\infty}^{\infty} S_k(\omega)d\omega \tag{3}$$

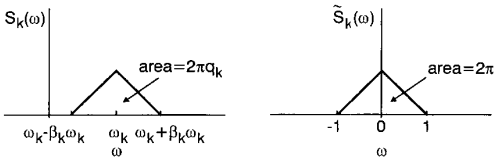

Fig. 1 *Example spectral density $S_k(\omega)$ of signal $s_k(t)$ and corresponding 'shape' spectral density $\tilde{S}_k(\omega)$*
Note that other shapes are possible (see Table 1)

The spectral density $S_k(\omega)$ is assumed to be a scaled and shifted version of a normalised 'shape' spectral density, denoted by $\tilde{S}_k(\omega)$, whose bandwidth (defined as half the width of the symmetric spectrum) is one and whose total power is one (the connection between the spectral density $S_k(\omega)$ and the 'shape' spectral density $\tilde{S}_k(\omega)$ is displayed in Fig. 1). This means that we assume the relation between $S_k(\omega)$ and $\tilde{S}_k(\omega)$ to be given by

$$S_k(\omega) = q_k \frac{1}{\beta_k\omega_k}\tilde{S}_k\left(\frac{\omega-\omega_k}{\beta_k\omega_k}\right) \tag{4}$$

In the case of a spectral density of finite support, the bandwidth of $S_k(\omega)$ is defined as

$$b_k \triangleq \beta_k\omega_k \tag{5}$$

where β_k is the relative bandwidth, with $0 \le \beta_k \le 1$. When the spectral density has infinite support (as, for example, in the case of $S_k(\omega)$ having a Gaussian shape) we can define an 'equivalent bandwidth' proportional to the square root of the second moment of $S_k(\omega)$:

$$b_k \triangleq \beta_k\omega_k = \left(\frac{1}{2\pi q_k}\int_{-\infty}^{\infty}\omega^2 S_k(\omega)d\omega\right)^{1/2} \tag{6}$$

(the second moment of $S_k(\omega)$ is assumed to be finite, which means that the $S_k(t)$ have finite energy).

To each source signal is associated a 'spectral shape' autocorrelation function $\tilde{r}_k(\tau)$, which is given by the inverse Fourier transform of $\tilde{S}_k(\omega)$. Thus $\tilde{r}_k(\tau)$ is normalised such that $\tilde{r}_k(0) = 1$. In addition, since $\tilde{S}_k(\omega)$ is assumed to have finite second moment, $\tilde{r}_k(\tau)$ is continuously differentiable at $\tau = 0$. The corresponding signal autocorrelation, $r_k(\tau)$, is found from eqn. 4 to b

$$r_k(\tau) = q_k e^{i\omega_k\tau}\cdot\tilde{r}_k(\beta_k\omega_k\tau) \tag{7}$$

As the relative bandwidth β_k approaches zero, $r_k(\tau) \to q_k e^{i\omega_k\tau}$ and $S_k(\omega) \to 2\pi q_k\delta(\omega-\omega_k)$, which are the autocorrelation and spectral density functions of a sinusoidal signal of frequency ω_k and power q_k, as desired.

The sampled array output at time t is the complex m-vector $\mathbf{x}(t) = [x_1(t), \ldots, x_m(t)]^T$, where the received signal at the μth sensor can be expressed as

$$x_\mu(t) = \sum_{k=1}^{n}\tilde{a}_\mu(\theta_k)s_k(t-T_{k\mu}) + n_\mu(t),\ \mu = 1,\ldots,m \tag{8}$$

where $T_{k\mu}$ is the time taken for the kth signal to propagate from an arbitrary reference point to the μth element of the array. The antenna elements' frequency responses are assumed to be constant amplitude and (identical) linear phase over the bandwidth of the source signals. This assumption, used also for bandwidth performance analysis of adaptive antenna systems [18], is valid for small relative bandwidths, which is the case of interest here. The linear phase term results in a constant time delay that can be included in the $T_{k\mu}$ terms. The remaining complex antenna gain terms are denoted $\tilde{a}_\mu(\theta)$, giving the array gain vector at angle θ

$$\tilde{\mathbf{a}}(\theta) = [\tilde{a}_1(\theta), \tilde{a}_2(\theta), \ldots, \tilde{a}_m(\theta)]^T \tag{9}$$

The $n_\mu(t)$ term in eqn. 8 is the noise component, and we assume that the noise vector $\mathbf{n}(t) = [n_1(t), \ldots, n_m(t)]^T$ is a zero mean, circularly complex random vector with $E\{\mathbf{n}(t)\mathbf{n}^*(s)\} = \lambda^2\mathbf{I}_m\delta_{t,s}$ and $E\{\mathbf{n}(t)\mathbf{n}^T(s)\} = 0$ (here * denotes the complex conjugate transpose).

If the source signals have zero bandwidth, i.e. if the usual narrowband assumption holds, a time delay of the signal can be modelled as a simple phase shift of the carrier. Then the array covariance matrix

$$\mathbf{R} \triangleq E\{\mathbf{x}(t)\mathbf{x}^*(t)\} \tag{10}$$

is given by the standard 'nominal' expression:

$$\mathbf{R}_0 = \mathbf{A}(\boldsymbol{\omega}_0, \boldsymbol{\theta}_0)\mathbf{Q}\mathbf{A}^*(\boldsymbol{\omega}_0, \boldsymbol{\theta}_0) + \lambda^2\mathbf{I}_m \tag{11}$$

where $\boldsymbol{\theta}_0 = [\theta_1, \ldots, \theta_n]^T$, $\boldsymbol{\omega}_0 = [\omega_1, \ldots, \omega_n]^T$, $\mathbf{A}(\boldsymbol{\omega}_0, \boldsymbol{\theta}_0) = [\mathbf{a}(\omega_1, \theta_1), \ldots, \mathbf{a}(\omega_n, \theta_n)]$ is the $m \times n$ array manifold matrix and $\mathbf{Q} = \mathrm{diag}\{q_1, \ldots, q_n\}$, where q_k is the received signal power from $s_k(t)$. Note that

$$\mathbf{a}(\omega_k, \theta_k) \triangleq \left[\tilde{a}_1(\theta_k)e^{-i\omega_k T_{k1}}, \ldots, \tilde{a}_m(\theta_k)e^{-i\omega_k T_{km}}\right]^T \tag{12}$$

For nonzero signal bandwidths, the (μ, ν)th element of the covariance matrix is given by

$$\begin{aligned} R(\mu,\nu) &= E\{x_\mu(t)x_\nu^*(t)\} \\ &= \sum_{k=1}^{n}\tilde{a}_\mu(\theta_k)\tilde{a}_\nu^*(\theta_k)r_k(T_{k\nu}-T_{k\mu}) + \lambda^2\delta_{\mu,\nu} \\ &= \sum_{k=1}^{n}a_\mu(\omega_k,\theta_k)q_k a_\nu^*(\omega_k,\theta_k) \\ &\qquad \times \tilde{r}_k(\beta_k\omega_k(T_{k\nu}-T_{k\mu})) + \lambda^2\delta_{\mu,\nu} \end{aligned} \tag{13}$$

where $a_\mu(\omega_k, \theta_k) = \tilde{a}_\mu(\theta_k)e^{-i\omega_k T_{k\mu}}$ (see eqn. 12). Eqn. 13 can be written in matrix form as

$$\mathbf{R} = \sum_{k=1}^{n} \left(\mathbf{a}(\omega_k, \theta_k) q_k \mathbf{a}^*(\omega_k, \theta_k) \odot \mathbf{B}_k \right) + \lambda^2 \mathbf{I}_m \quad (14)$$

where $\odot$ denotes the Hadamard (element-wise) product. The $m \times m$ matrices $\{\mathbf{B}_k\}_{k=1}^n$ are defined by their (μ, ν)th elements:

$$\mathbf{B}_k(\mu, \nu) = \tilde{r}_k \left(\beta_k \omega_k (T_{k\nu} - T_{k\mu}) \right) \quad (15)$$

(the result (eqn. 14) is also presented in a different form in [1]). For $\beta_k = 0$, $\mathbf{B}_k$ is a matrix whose elements are all ones, and $\mathbf{R}$ reduces to $\mathbf{R}_0$ in eqn. 11.

3 Small perturbation properties of R

We now assume that the fractional bandwidths β_k are 'small' and find the Taylor series expansion of $\mathbf{R}$ as a function of $\boldsymbol{\beta} = [\beta_1, \ldots \beta_n]$ about the nominal covariance $\mathbf{R}_0$, and retain terms up to and including second order in $\boldsymbol{\beta}$. Because only $\mathbf{B}_k$ in eqn. 14 depends on β_k, we need only the Taylor series expansion of $\tilde{r}_k(\omega_k \beta_k \tau)$ about the point $\beta_k = 0$. We have

$$\frac{\partial \mathbf{R}}{\partial \beta_k} = \mathbf{a}(\omega_k, \theta_k) q_k \mathbf{a}^*(\omega_k, \theta_k) \odot \frac{\partial \mathbf{B}_k}{\partial \beta_k} \quad (16)$$

and

$$\frac{\partial^2 \mathbf{R}}{\partial \beta_k \partial \beta_l} = \begin{cases} \mathbf{a}(\omega_k, \theta_k) q_k \mathbf{a}^*(\omega_k, \theta_k) \odot \frac{\partial^2 \mathbf{B}_k}{\partial \beta_k^2} & k = l \\ 0 & k \neq l \end{cases} \quad (17)$$

(there are no crossterms in the expansion as the sources are assumed to be independent). The covariance matrix in eqn. 14 can thus be expanded as

$$\mathbf{R} \simeq \mathbf{R}_0 + \sum_{k=1}^{n} \left[\beta_k \tilde{\mathbf{C}}_k + \beta_k^2 \tilde{\mathbf{B}}_k \right] = \mathbf{R}_0 + \tilde{\mathbf{C}} + \tilde{\mathbf{B}} \quad (18)$$

where the (μ, ν)th elements of $\tilde{\mathbf{C}}_k$ and $\tilde{\mathbf{B}}_k$ are given by

$$\tilde{\mathbf{C}}_k(\mu, \nu) = a_\mu(\omega_k, \theta_k) q_k a_\nu^*(\omega_k, \theta_k) \times \left[\frac{\partial}{\partial \beta_k} \tilde{r}_k \left(\omega_k \beta_k (T_{k\nu} - T_{k\mu}) \right) \Big|_{\beta_k = 0} \right] \quad (19)$$

$$\tilde{\mathbf{B}}_k(\mu, \nu) = \frac{1}{2} a_\mu(\omega_k, \theta_k) q_k a_\nu^*(\omega_k, \theta_k) \times \left[\frac{\partial^2}{\partial \beta_k^2} \tilde{r}_k \left(\omega_k \beta_k (T_{k\nu} - T_{k\mu}) \right) \Big|_{\beta_k = 0} \right] \quad (20)$$

Through the Fourier-pair relation between $\tilde{r}_k(\tau)$ and $\tilde{S}_k(\omega)$ and since $\tilde{S}_k(\omega)$ is symmetric, we have

$$\tilde{r}_k'(\tau)\Big|_{\tau=0} = \lim_{\tau \to 0} \frac{1}{2\pi} \int_{-\infty}^{\infty} i\omega \tilde{S}_k(\omega) e^{i\omega\tau} d\omega = \frac{1}{2\pi} \int_{-\infty}^{\infty} i\omega \tilde{S}_k(\omega) d\omega = 0 \quad (21)$$

Since

$$\frac{\partial}{\partial \beta_k} \tilde{r}_k \left(\omega_k \beta_k (T_{k\nu} - T_{k\mu}) \right) \Big|_{\beta_k = 0} = (T_{k\nu} - T_{k\mu}) \omega_k \tilde{r}_k'(\tau) \Big|_{\tau=0} = 0 \quad (22)$$

it follows that $\tilde{\mathbf{C}}_k \equiv 0$. We also have that

$$\frac{\partial^2}{\partial \beta_k^2} \tilde{r}_k \left(\omega_k \beta_k (T_{k\nu} - T_{k\mu}) \right) \Big|_{\beta_k = 0} = (T_{k\nu} - T_{k\mu})^2 \omega_k^2 \tilde{r}_k''(\tau) \Big|_{\tau=0} \triangleq (T_{k\nu} - T_{k\mu})^2 \omega_k^2 \kappa_k \quad (23)$$

where $\kappa_k \triangleq \tilde{r}_k''(0)$. The same kind of argument as above gives

$$\kappa_k = \lim_{\tau \to 0} \frac{1}{2\pi} \int_{-\infty}^{\infty} -\omega^2 \tilde{S}_k(\omega) e^{i\omega\tau} d\omega = \frac{1}{2\pi} \int_{-\infty}^{\infty} -\omega^2 \tilde{S}_k(\omega) d\omega \quad (24)$$

The integral in eqn. 24 is well defined since $\tilde{S}_k(\omega)$ is assumed to have a finite second moment. To summarise, for a symmetric spectral density

$$\mathbf{R} \simeq \mathbf{R}_0 + \sum_{k=1}^{n} \beta_k^2 \tilde{\mathbf{B}}_k = \mathbf{R}_0 + \tilde{\mathbf{B}} \quad (25)$$

where the (μ, ν)th element of $\tilde{\mathbf{B}}_k$ is given by

$$\tilde{\mathbf{B}}_k(\mu, \nu) = \frac{1}{2} a_\mu(\omega_k, \theta_k) q_k a_\nu^*(\omega_k, \theta_k) (T_{k\nu} - T_{k\mu})^2 \omega_k^2 \kappa_k \quad (26)$$

A few examples of spectral shape models, together with their normalised autocorrelation functions and κ_k values, are given in Table 1.

4 Perturbation analysis of DOA estimators

We analyse the error of DOA estimators when the source signals have small but nonzero bandwidth. The approach we take is to perform a small perturbation analysis of the estimation algorithms, using the

Table 1: Examples of some spectral density models and their corresponding normalised autocorrelation functions

	$\tilde{S}_k(\omega)$	$\tilde{r}_k(\tau)$	κ_k
E.1	$\begin{cases} \pi & \lvert\omega\rvert \le 1 \\ 0 & \text{elsewhere} \end{cases}$	$\operatorname{sinc} \tau$	−1/3
E.2	$\begin{cases} \pi(1 + \cos(\pi\omega)) & \lvert\omega\rvert \le 1 \\ 0 & \text{elsewhere} \end{cases}$	$\pi^2 \operatorname{sinc} \tau / (\pi^2 - \tau^2)$	$2[(1/\pi^2) - (1/6)]$
E.3	$\begin{cases} 2\pi(-\lvert\omega\rvert + 1) & \lvert\omega\rvert \le 1 \\ 0 & \text{elsewhere} \end{cases}$	$2(1 - \cos \tau)/\tau^2$	−1/6
E.4	$\sqrt{(2\pi)} \exp(-\omega^2/2)$	$\lvert\omega\rvert \le \infty$ $\exp(-\tau^2/2)$	−1

$\operatorname{sinc} x \triangleq (\sin x)/x$; E.1 = flat spectrum; E.2 = raised cosine spectrum; E.3 = triangular spectrum; E.4 = Gaussian spectrum

perturbation results on $\mathbf{R}$ obtained above (and on its corresponding sample estimate $\hat{\mathbf{R}}$).

4.1 Signal and noise subspaces

In practice, the true covariance matrix $\mathbf{R}$ is not available and must be estimated from a sample of N data points of the array output, $\{\mathbf{x}(t)\}_{t=1}^{N}$, according to

$$\hat{\mathbf{R}} = \frac{1}{N}\sum_{t=1}^{N}\mathbf{x}(t)\mathbf{x}^*(t) \tag{27}$$

If the elements of $\mathbf{x}(t)$ are given by eqn. 8, then we can write

$$\begin{aligned}\hat{\mathbf{R}} &\simeq \mathbf{R}_0 + \sum_{k=1}^{n}\beta_k^2\tilde{\mathbf{B}}_k + \tilde{\mathbf{M}} \\ &= \mathbf{R}_0 + \tilde{\mathbf{B}} + \tilde{\mathbf{M}}\end{aligned} \tag{28}$$

where the matrices $\tilde{\mathbf{B}}_k$ are given by eqn. 26 and where $\tilde{\mathbf{M}}$ is a random perturbation (of order $1/N$) on $\mathbf{R}$ due to the finite sample size N. Consider the following subspace decompositions of $\mathbf{R}_0$ and $\hat{\mathbf{R}}$:

$$\mathbf{R}_0 = \mathbf{S}\Lambda\mathbf{S}^* + \lambda^2\mathbf{G}\mathbf{G}^* \tag{29}$$

$$\hat{\mathbf{R}} = \hat{\mathbf{S}}\hat{\Lambda}\hat{\mathbf{S}}^* + \hat{\mathbf{G}}\hat{\Sigma}\hat{\mathbf{G}}^* \tag{30}$$

where $\Lambda = \mathrm{diag}\{\lambda_1 \ldots \lambda_n\}$ contains the n largest eigenvalues of $\mathbf{R}_0$, $\mathbf{S}$ is the corresponding matrix of the n associated orthonormal eigenvectors, and $\mathbf{G}$ is the matrix of the remaining $m - n$ orthonormal eigenvectors (we assume that $\{\lambda_i\}_{i=1}^{n}$ are distinct and greater than λ^2). The matrices $\hat{\mathbf{S}}$, $\hat{\Lambda}$, $\hat{\mathbf{G}}$ and $\hat{\Sigma}$ are the estimated counterparts of $\mathbf{S}$, Λ, $\mathbf{G}$ and Σ. Then as $\beta_k \to 0$ and $N \to \infty$, we have $\hat{\mathbf{R}} \to \mathbf{R}_0$, $\hat{\mathbf{S}} \to \mathbf{S}$, $\hat{\Lambda} \to \Lambda$, $\hat{\Sigma} \to \lambda^2\mathbf{I}_{m-n}$ and $\hat{\mathbf{G}}\hat{\mathbf{G}}^* \to \mathbf{G}\mathbf{G}^*$ [19].

Define $\mathring{\Lambda} \triangleq \Lambda - \lambda^2\mathbf{I}_n (n \times n)$ and let $P_A \triangleq \mathbf{A}(\mathbf{A}^*\mathbf{A})^{-1}\mathbf{A}^* = \mathbf{A}\mathbf{A}^\dagger$ and $P_A^\perp \triangleq \mathbf{I} - P_A$ denote the projection matrices onto the range and null spaces of a matrix $\mathbf{A}$ (where $\mathbf{A}^\dagger = (\mathbf{A}^*\mathbf{A})^{-1}\mathbf{A}^*$ is the pseudo-inverse of $\mathbf{A}$). To simplify the notation, in what follows we often write $\mathbf{a}_k$ instead of $\mathbf{a}(\omega_k, \theta_k)$ and $\mathbf{d}_k$ instead of $\partial\mathbf{a}_k/\partial\theta_k$.

4.2 MUSIC algorithm

The MUSIC algorithm gives the DOA estimates $\{\hat{\theta}_k^M\}_{k=1}^{n}$ as the n largest maxima of the scalar function

$$\hat{V}_M(\theta) = \mathrm{tr}\left\{\mathbf{P}_{\mathbf{a}(\theta)}\hat{\mathbf{S}}\hat{\mathbf{S}}^*\right\} \tag{31}$$

Expanding the gradient $\hat{V}_M'(\theta) \triangleq \partial/\partial\theta\ \hat{V}_M(\theta)$ in a Taylor series about the true angle of arrival $\theta_k = \theta_k$, $k = 1, \ldots, n$, gives to first order

$$\hat{\theta}_k^M - \theta_k = -\left[V''(\theta_k)\right]^{-1}\hat{V}_M'(\theta_k) \tag{32}$$

where $V''(\theta) \triangleq \partial^2/\partial\theta^2\ \hat{V}_M(\theta)$ is the Hessian of $\hat{V}_M(\theta)$. Defining $\tilde{\mathbf{G}} = \hat{\mathbf{G}} - \mathbf{G}$ and $\tilde{\Sigma} = \hat{\Sigma} - \Sigma$ and carrying through the calculations yield

$$\begin{aligned}\hat{V}_M'(\theta_k) &= \mathrm{tr}\left\{\frac{\partial\mathbf{P}_{\mathbf{a}(\theta)}}{\partial\theta}\hat{\mathbf{S}}\hat{\mathbf{S}}^*\right\}\Bigg|_{\theta=\theta_k} \\ &= 2\mathrm{Re}\left\{\mathrm{tr}\left[\mathbf{P}_{\mathbf{a}_k}^\perp\mathbf{d}_k\mathbf{a}_k^\dagger\hat{\mathbf{S}}\hat{\mathbf{S}}^*\right]\right\} \\ &= 2\mathrm{Re}\left\{\mathbf{a}_k^\dagger(\mathbf{I} - \hat{\mathbf{G}}\hat{\mathbf{G}}^*)\mathbf{P}_{\mathbf{a}_k}^\perp\mathbf{d}_k\right\} \\ &\simeq -2\mathrm{Re}\left\{\mathbf{a}_k^\dagger\tilde{\mathbf{G}}\mathbf{G}^*\mathbf{d}_k\right\}\end{aligned} \tag{33}$$

where we have used the fact that $\mathbf{G}^*\mathbf{P}_{\mathbf{a}_k}^\perp = \mathbf{G}^*$ and where the approximation is valid as $N \to \infty$. We aim at expressing the error in terms of the covariance matrix (eqn. 28) rather than in terms of the noise subspace as in eqn. 33. To that end, the following derivation is useful:

$$\begin{aligned}&\hat{\mathbf{R}}\hat{\mathbf{G}} = \hat{\mathbf{G}}\hat{\Sigma} \\ &\Longrightarrow \mathbf{R}_0\tilde{\mathbf{G}} + \hat{\mathbf{R}}\mathbf{G} \simeq \sigma^2\tilde{\mathbf{G}} + \mathbf{G}\tilde{\Sigma} + \sigma^2\mathbf{G} \\ &\Longrightarrow \mathbf{S}^*\mathbf{R}_0\tilde{\mathbf{G}} + \mathbf{S}^*\hat{\mathbf{R}}\mathbf{G} \simeq \sigma^2\mathbf{S}^*\tilde{\mathbf{G}} \\ &\Longrightarrow \mathbf{S}^*\hat{\mathbf{R}}\mathbf{G} \simeq -\mathring{\Lambda}\mathbf{S}^*\tilde{\mathbf{G}} \\ &\Longrightarrow -\mathbf{a}_k^\dagger\mathbf{S}\mathring{\Lambda}^{-1}\mathbf{S}^*\hat{\mathbf{R}}\mathbf{G} \simeq \mathbf{a}_k^\dagger\mathbf{S}\mathbf{S}^*\tilde{\mathbf{G}} = \mathbf{a}_k^\dagger\tilde{\mathbf{G}}\end{aligned} \tag{34}$$

Combining eqns. 33 and 34 and using eqn. 28 we obtain

$$\begin{aligned}&\hat{V}_M'(\theta_k) \\ &\quad\simeq 2\mathrm{Re}\left\{(\mathbf{a}_k^*\mathbf{a}_k)^{-1}\mathbf{a}_k^*\mathbf{S}\mathring{\Lambda}^{-1}\mathbf{S}^*[\tilde{\mathbf{B}} + \tilde{\mathbf{M}}]\mathbf{G}\mathbf{G}^*\mathbf{d}_k\right\}\end{aligned} \tag{35}$$

In the same manner, it is possible to show that for $V_M''(\theta_k)$ we have

$$\begin{aligned}V_M''(\theta_k) &= \mathrm{tr}\left\{\frac{\partial^2\mathbf{P}_{\mathbf{a}(\theta)}}{\partial\theta^2}\mathbf{S}\mathbf{S}^*\right\}\Bigg|_{\theta=\theta_k} \\ &= 2\mathrm{Re}\left\{\frac{\partial\mathbf{a}_k^\dagger}{\partial\theta_k}\mathbf{S}\mathbf{S}^*\mathbf{P}_{\mathbf{a}_k}^\perp\mathbf{d}_k - \mathbf{a}_k^\dagger\mathbf{S}\mathbf{S}^*\frac{\partial\mathbf{P}_{\mathbf{a}_k}}{\partial\theta_k}\mathbf{d}_k\right\} \\ &= 2\mathrm{Re}\left\{(\mathbf{a}_k^*\mathbf{a}_k)^{-1}\mathbf{d}_k^*\mathbf{S}\mathbf{S}^*\mathbf{P}_{\mathbf{a}_k}^\perp\mathbf{d}_k\right. \\ &\qquad\left. -(\mathbf{a}_k^*\mathbf{a}_k)^{-1}\mathbf{d}_k^*\mathbf{P}_{\mathbf{a}_k}^\perp\mathbf{d}_k\right\} \\ &= -2(\mathbf{a}_k^*\mathbf{a}_k)^{-1}\mathbf{d}_k^*\mathbf{G}\mathbf{G}^*\mathbf{d}_k\end{aligned} \tag{36}$$

Combining eqns. 35 and 36 we obtain that the MUSIC error, to second order in β_k, is given by

$$\begin{aligned}&\hat{\theta}_k^M - \theta_k \\ &\quad\simeq \frac{\mathrm{Re}\left\{\mathbf{a}_k^*\mathbf{S}\mathring{\Lambda}^{-1}\mathbf{S}^*\left[\sum_{i=1}^{n}\beta_i^2\tilde{\mathbf{B}}_i + \tilde{\mathbf{M}}\right]\mathbf{G}\mathbf{G}^*\mathbf{d}_k\right\}}{\mathbf{d}_k^*\mathbf{G}\mathbf{G}^*\mathbf{d}_k}\end{aligned} \tag{37}$$

$$\triangleq \sum_{i=1}^{n}\beta_i^2 b_{ik}^M + \tilde{\theta}_k^M, \quad k = 1, \ldots, n \tag{38}$$

Eqn. 37 could also be found by using results in [20] on the first-order expansion of the projection matrix $\mathbf{P} = \hat{\mathbf{S}}\hat{\mathbf{S}}^*$, together with results on the derivatives of a non-normalised version of the MUSIC cost function, eqn. 31 (see [21]). We chose to give the derivation above as it is also valid for the WSF algorithm, as will be indicated below.

4.3 ESPRIT algorithm

The ESPRIT algorithm [22] assumes that the array can be partitioned into two subsets. The two subarrays are identical except for a translational shift of Δ wavelengths. In terms of the array manifold matrix, this assumption can be written

$$\mathbf{A}_1 = [\mathbf{I}_m \quad 0]\mathbf{A} \qquad \mathbf{A}_2 = [0 \quad \mathbf{I}_m]\mathbf{A} \tag{39}$$

where $\mathbf{A}_1$ and $\mathbf{A}_2$ are the manifolds for the two subarrays, respectively. Define the matrices

$$\mathbf{S}_1 = [\mathbf{I}_m \quad 0]\mathbf{S} \qquad \mathbf{S}_2 = [0 \quad \mathbf{I}_m]\mathbf{S} \tag{40}$$

$$\phi = (\mathbf{S}_1^*\mathbf{S}_1)^{-1}\mathbf{S}_1^*\mathbf{S}_2 \tag{41}$$

and similarly $\hat{\mathbf{S}}_1$, $\hat{\mathbf{S}}_2$ and $\hat{\boldsymbol{\phi}}$. If $\{\rho_k\}_{k=1}^n$ and $\{\hat{\rho}_k\}_{k=1}^n$ are the eigenvalues of the matrices $\boldsymbol{\phi}$ and $\hat{\boldsymbol{\phi}}$, respectively, then the DOA estimates of the ESPRIT algorithm [22] are given by

$$\hat{\theta}_k^E = \sin^{-1}\left(\frac{\arg\hat{\rho}_k}{2\pi\Delta}\right), \quad k = 1, \ldots, n \tag{42}$$

where the shift-invariance of the array has been used. It follows that

$$\hat{\theta}_k^E - \theta_k^E \simeq \frac{1}{2\pi\Delta\cos\theta_k}\mathrm{Im}\left\{\frac{\hat{\rho}_k - \rho_k}{\rho_k}\right\} \tag{43}$$

Let $\{\boldsymbol{\gamma}_k^*\}$ and $\{\boldsymbol{\eta}_k\}$ denote the left and right eigenvectors of $\boldsymbol{\phi}$, normalised so that $\boldsymbol{\gamma}_k^*\boldsymbol{\eta}_k = 1$. Introduce $\boldsymbol{\mu}_k^* = \boldsymbol{\gamma}_k^*(\mathbf{S}_1^*\mathbf{S}_1)^{-1}\mathbf{S}_1^*\{[0\ \mathbf{I}_m] - \rho_k[\mathbf{I}_m\ 0]\}$. Then it is shown in [14] that

$$\hat{\rho}_k - \rho_k \simeq \boldsymbol{\mu}_k^*\mathbf{G}\mathbf{G}^*\hat{\mathbf{S}}\boldsymbol{\eta}_k \tag{44}$$

Using eqns. 43 and 44 together with eqn. 28 we obtain, to second order in β_k, the ESPRIT error

$$\hat{\theta}_k^E - \theta_k \simeq \frac{1}{2\pi\Delta\cos\theta_k} \times\mathrm{Im}\left\{\frac{1}{\rho_k}\boldsymbol{\mu}_k^*\mathbf{G}\mathbf{G}^*\left[\sum_{i=1}^n \beta_i^2\tilde{\mathbf{B}}_i + \tilde{\mathbf{M}}\right]\mathbf{S}\mathring{\mathbf{\Lambda}}^{-1}\boldsymbol{\eta}_k\right\} \tag{45}$$

$$\triangleq \sum_{i=1}^n \beta_i^2 b_{ik}^E + \tilde{\theta}_k^E \tag{46}$$

4.4 WSF algorithm

The WSF algorithm computes the DOA estimates as the vector $\hat{\boldsymbol{\theta}}^W$ that maximises a scalar loss function (of a vector variable), i.e.

$$\hat{\boldsymbol{\theta}}^W = \arg\max \hat{V}(\boldsymbol{\theta}) \tag{47}$$

where $\hat{\boldsymbol{\theta}}^W = [\hat{\theta}_1{}^W, \ldots, \hat{\theta}_n{}^W]^T$ is the vector of WSF DOA estimates and

$$\hat{V}(\boldsymbol{\theta}) = \mathrm{tr}\left\{\mathbf{P}_{\mathbf{A}(\boldsymbol{\theta})}\hat{\mathbf{S}}\mathbf{W}\hat{\mathbf{S}}^*\right\} \tag{48}$$

This loss function is a multidimensional counterpart of the scalar MUSIC criterion, eqn. 31. The matrix $\mathbf{W}$ included in eqn. 48 is a positive definite and Hermitian weighting matrix that can be chosen by the user. Using the same kind of derivation as in Section 4.2, we obtain (to second order in β_k) the WSF error

$$\hat{\boldsymbol{\theta}}^W - \boldsymbol{\theta}_0 \simeq \left\{2\mathrm{Re}[\mathbf{A}^\dagger\mathbf{S}\mathbf{W}\mathbf{S}^*\mathbf{A}^{\dagger *} \odot \mathbf{D}^*\mathbf{G}\mathbf{G}^*\mathbf{D}]\right\}^{-1}\hat{\mathbf{V}}'(\boldsymbol{\theta}_0) \tag{49}$$

with $\mathbf{D} = [\mathbf{d}_1, \ldots, \mathbf{d}_n]$ and where $\hat{\mathbf{V}}'(\boldsymbol{\theta})$, the gradient vector of $\hat{\mathbf{V}}(\boldsymbol{\theta})$, has the kth element

$$\hat{\mathbf{V}}_k'(\boldsymbol{\theta}_0) \simeq 2\mathrm{Re}\left\{\mathbf{e}_k^T\mathbf{A}^\dagger\mathbf{S}\mathbf{W}\mathring{\mathbf{\Lambda}}^{-1}\mathbf{S}^*\left[\sum_{i=1}^n \beta_i^2\tilde{\mathbf{B}}_i + \tilde{\mathbf{M}}\right]\mathbf{G}\mathbf{G}^*\mathbf{d}_k\right\} \tag{50}$$

($\mathbf{e}_k$ is the column vector containing only zeros except for having 1 as its kth element). Again, the error can be expressed as the sum

$$\hat{\boldsymbol{\theta}}^W - \boldsymbol{\theta}_0 \simeq \sum_{i=1}^n \beta_i^2\mathbf{b}_i^W + \tilde{\boldsymbol{\theta}}^W \tag{51}$$

4.5 DOA error: deterministic and random components

Eqns. 38, 46 and 51 give the error induced by a nonzero bandwidth for the MUSIC, ESPRIT and WSF algorithms, respectively. As can be seen from these equations, the second-order error is the sum of two terms. The first term is the error induced by the nonzero bandwidth of the signals. Each b_{ik} represents the error in the kth DOA estimate induced by the ith source. Thus, a DOA estimate $\hat{\boldsymbol{\theta}}$ derived from $\hat{\mathbf{R}}$ can, under mild conditions, be written as

$$\hat{\boldsymbol{\theta}} \simeq \boldsymbol{\theta}_0 + \underbrace{\mathbf{b}}_{O(\beta_k^2)} + \underbrace{\tilde{\boldsymbol{\theta}}}_{O(1\sqrt{N})} \tag{52}$$

In eqn. 52, $\mathbf{b}$ is the second-order error due to nonzero bandwidth (i.e. corresponding to $\tilde{\mathbf{B}}$). The second term, $\tilde{\boldsymbol{\theta}}_k$, is the large-sample estimation error (i.e. corresponding to $\tilde{\mathbf{M}}$). It follows from eqn. 52 that the mean-squared error is

$$E\{\hat{\boldsymbol{\theta}}\hat{\boldsymbol{\theta}}^T\} - \boldsymbol{\theta}_0\boldsymbol{\theta}_0^T \simeq \underbrace{\mathbf{b}\mathbf{b}^T}_{O(\beta_k^4)} + \underbrace{\mathrm{cov}(\tilde{\boldsymbol{\theta}})}_{O(1/N)} + \underbrace{\mathbf{b}E\{\tilde{\boldsymbol{\theta}}\}^T + E\{\tilde{\boldsymbol{\theta}}\}\mathbf{b}^T}_{O(\beta_k^2\cdot 1/N)} \tag{53}$$

The first term in eqn. 53 is the square of the deterministic error due to nonzero bandwidth. The second term is the variance of the DOA estimate for the nominal case of narrowband source signals. This variance has been well studied in the literature, and expressions for the large-sample variance of $\tilde{\boldsymbol{\theta}}$ are known when $\beta_k \equiv 0$; see, for example, [4–10] (for the case of small N, see [23]). These studies show that $\tilde{\boldsymbol{\theta}}$ has mean of $O(1/N)$ and a standard deviation of $O(1/\sqrt{N})$ for large N. Thus, we obtain the magnitude order expressions as shown in eqn. 53. The final term in eqn. 53 shows a linear increase in the variance of the DOA estimate as a function of $\beta_k{}^2$, with slope given by $E\{\tilde{\boldsymbol{\theta}}\}$. We note that for both $\beta_k{}^2$ and $1/N$ 'small', the last term in eqn. 53, is negligible with respect to the first two terms. In view of the above observations, it is clear that if $\beta_k{}^2 >> 1/\sqrt{N}$, then the bandwidth-induced error dominates the error due to finite sample effects.

4.6 Uniform linear array and a single source

The complex array response for the μth element of a uniform linear array (ULA) with an interelement spacing of Δ wavelengths is given by

$$a_\mu(\omega, \theta) = e^{2\pi i\Delta(\mu-1)\sin(\theta)} \tag{54}$$

For a scenario with a single source impinging on a ULA, it is readily shown that the bandwidth-induced error (to second order in β_k) is zero for all the algorithms considered here.

5 Numerical examples

In this Section we present some numerical examples that illustrate the effect of nonzero bandwidth on the DOA estimators. We restrict our attention to the case of a uniform linear array. Thus, the complex array response of the μth sensor to a signal arriving from an angle θ is given by eqn. 54, where the incident angle is measured from the broadside of the array. We consider the case of two signals impinging from different directions on an array of m sensors with half-wavelength spacing. The signals each have a flat spectrum, the

expression of which is given by example E.1 of Table 1, and arrive at angles θ_1 and θ_2. The centre frequencies ω_1 and ω_2 are assumed to be equal, as are the relative bandwidths β_1 and β_2.

We present the results mainly for the MUSIC algorithm, but the results are very similar for ESPRIT and WSF. In the Figures we compare the 'true' ($N = \infty$) error, obtained by applying the algorithms to the covariance matrix in eqn. 14 to the one obtained by the above second-order theory. Note that (except for Fig. 8) we do not include the effect of noise in the simulations, i.e. we have $\lambda^2 = 0$ in eqn. 14. The reason is to isolate the effect of the bandwidth-induced error. With no noise (or infinite samples), it is clear that whatever error is present in the DOA estimates is due to the signal bandwidth only, which is the error we are attempting to quantify.

Fig. 2 shows the error of the MUSIC algorithm as a function of the array size m. The two sources have equal power and impinge on the array from the angles $\theta_1 = 20°$ and $\theta_2 = 50°$ with relative bandwidths $\beta_1 = \beta_2 = 0.1$. The first-order theory predicts the error accurately for small array sizes ($m \leq 20$ in this example). As seen in Fig. 2, the error becomes very small for a large value of m, and in what follows we focus on 'small' arrays.

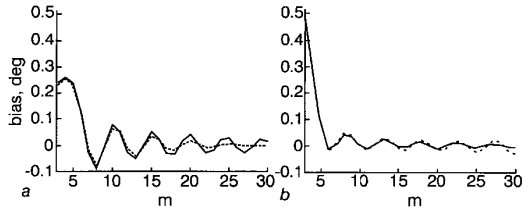

Fig. 2 *MUSIC estimation error as a function of array size m for two sources of equal power impinging from $\theta_1 = 20°$ and $\theta_2 = 50°$ with relative bandwidth $\beta_1 = \beta_2 = 0.1$*
——— first order
- - - - true
a Source 1
b Source 2

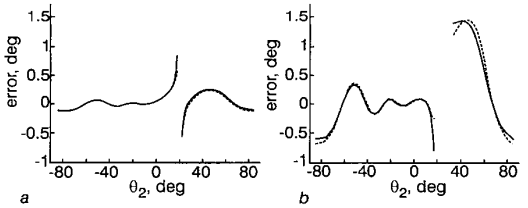

Fig. 3 *MUSIC estimation error for a source impinging from $\theta_1 = 20°$ as a function of DOA of second source for cases of equal power and of relative power $q_2/q_1 = 5$*
$\beta_1 = \beta_2 = 0.1$ and $m = 5$
a Sources of equal power
b Sources of different power
——— first order
- - - - true

Figs. 3–5 show the error of a source fixed at $\theta_1 = 20°$ when the DOA of the second source is varied from –85° to 85°; the relative bandwidths are $\beta_1 = \beta_2 = 0.1$ and $m = 5$. Figs. 3*a* and *b* show the results for MUSIC for the cases when the sources have equal power and when the sources have a relative power of $q_2/q_1 = 5$, respectively. When θ_2 is close to 20° the sources are not well separated, and we see that the error increases significantly in this high resolution scenario. Also, the error increases significantly even for a moderate difference in the source powers, a fact also noted in the presence of multipath induced angular spread [16]. This can be explained by the corresponding eigenvalue spread. As the bandwidth increases, the number of dominant eigenvalues increases, and due to the so-called 'leakage' of power, the signal subspace loses dimension (see [1]).

In Figs. 4 and 5 the corresponding results for the ESPRIT and WSF algorithms are shown (for the WSF algorithm we have chosen the weighting $\mathbf{W} = \hat{\mathbf{\Lambda}}^2\hat{\mathbf{\Lambda}}^{-1}$, which is known to minimise the variance of the DOA estimates due to finite sample effects). The error is slightly larger for ESPRIT than for the MUSIC and WSF algorithms. This is, indeed, expected since the use of the shift-invariance property of the array corresponds to the 'loss' of one sensor.

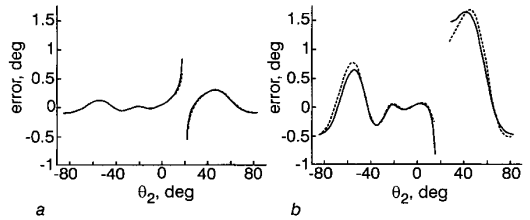

Fig. 4 *ESPRIT estimation error for a source impinging from $\theta_1 = 20°$ as a function of DOA of second source for cases of equal power and of relative power $q_2/q_1 = 5$*
$\beta_1 = \beta_2 = 0.1$ and $m = 5$
a Sources of equal power
b Sources of different power
· · · · first order
- - - - true

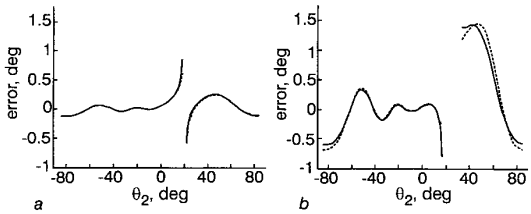

Fig. 5 *WSF estimation error for a source impinging from $\theta_1 = 20°$ as a function of DOA of second source for cases of equal power and of relative power $q_2/q_1 = 5$*
$\beta_1 = \beta_2 = 0.1$ and $m = 5$
a Sources of equal power
b Sources of different power
· · · · first order
- - - - true

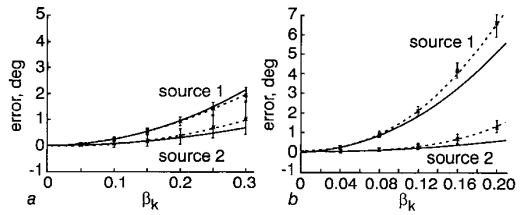

Fig. 6 *MUSIC estimation error and 1 standard deviation error bars as a function of relative bandwidth for two sources fixed at $\theta_1 = 20°$ and $\theta_2 = 50°$ for the cases of equal and different powers: $q_2/q_1 = 5$ ($m = 5$)*
Note that scales are different in the two Figures
· · · · first order
- - - - true R
✳ simulated
N = 1000
a Sources of equal power
b Sources of different power

Fig. 6 shows the MUSIC error of two sources fixed at $\theta_1 = 20°$ and $\theta_2 = 50°$, as a function of the relative bandwidth for $m = 5$. The cases of equal and different source powers ($q_2/q_1 = 5$) are depicted in Figs. 6*a* and

b, respectively. Fig. 6b indicates that the error in the estimate of the DOA of a weak source can become significant even for small relative bandwidths (note the difference in the scale between the two Figures).

Fig. 6 also shows the effect of a finite sample signal (N = 1000). A truncated waveform does not have exactly the power spectral density assumed in the analysis. Thus, in addition to the approximation error due to dropping terms of order > β^2, there is an additional error due to the use of finite length data. This error will be different for each realisation in a Monte Carlo simulation. In Fig. 6 we have plotted the mean together with 1 standard deviation bars for 100 Monte Carlo runs. We see that the standard deviation due to finite samples is smaller than or of the same magnitude as the error induced by the nonzero bandwidth.

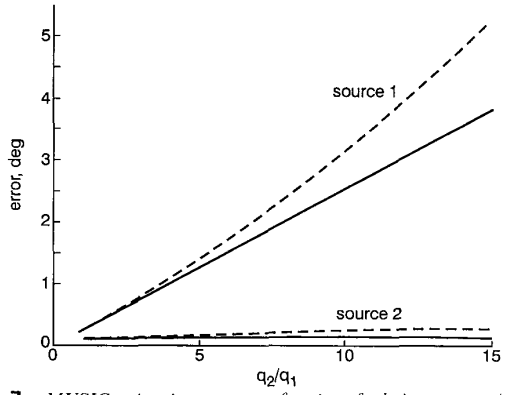

Fig. 7 *MUSIC estimation error as a function of relative power q_2/q_1 for $\theta_1 = 20°$, $\theta_2 = 50°$, $\beta_1 = \beta_2 = 0.1$ and $m = 5$*
——·· first order
– – – true

Fig. 7 shows the MUSIC error of two sources fixed at θ_1 = 20° and θ_2 = 50°, as a function of relative power q_2/q_1. The sources have relative bandwidth β_1 = β_2 = 0.1 and m = 5. The error predicted by the first-order theory, being linear in q_2/q_1, is accurate only for small values of the relative power. Again, we note that the true error for the weak source increases rapidly as the power of the second source increases. If the relative power becomes very large, the MUSIC algorithm completely fails to resolve the two sources.

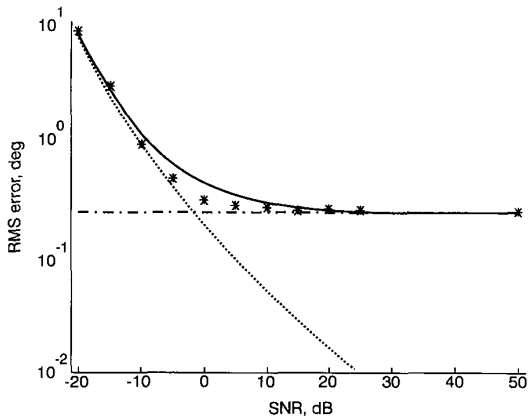

Fig. 8 *Root-mean-square (RMS) error for MUSIC as a function of SNR for $\theta_1 = 20°$, $\theta_2 = 50°$, $\beta_1 = \beta_2 = 0.1$, $m = 5$ and $N = 1000$ together with first-order bandwidth-induced error and RMS error due to noise only*
* simulation
····· noise error
·–·–· 1st-order bandwidth error
——— bandwidth and noise errors

Fig. 8 shows the root-mean-square (RMS) error for the MUSIC algorithm (calculated from 100 independent Monte Carlo runs) as a function of SNR and shows the corresponding analytical error predictions. Again m = 5, and the two equally powered sources are located at θ_1 = 20° and θ_2 = 50° and have relative bandwidth β_1 = β_2 = 0.1 (the Figure shows the error in the estimation in θ_2). A sample length of N = 1000 is used in the simulation. At high SNR, the effects of signal bandwidth dominate, and the RMS error approaches the error predicted by the theoretical results. For low SNR, the effects of noise dominate, and the RMS error is close to that due to noise only, as given, for example, in [24].

6 Conclusions

In this paper we have analysed the effect of a small but nonzero bandwidth on narrowband DOA estimation. We have presented analytical expressions for the resulting error, and illustrated our results by means of some numerical examples. We have found that the bandwidth-induced error, while small for many cases of interest, may become significant in difficult scenarios, such as when the source signals are closely spaced in angle or have a large difference in power.

7 Acknowledgment

This work has been supported by grants from the Swedish Institute, by NUTEK under project number 93-03103, and by the US Army Research Laboratory under contract DAAL01-93-C-0095.

8 References

1 NICKEL, U.: 'On the influence of channel errors on arrray signal processing methods', *Arch. Elektron. Übertrag. (Int. J. Electron. Commun.)*, 1993, **AEÜ–47**, (4), pp. 209–219
2 SCHULTHEISS, P.M., and MESSER, H.: 'Optimal and suboptimal broad-band source location estimation', *IEEE Trans. Signal Process.*, 1993, **41**, pp. 2752–2763
3 LEE, T.-S.: 'Efficient wide-band source localization using beamforming invariance technique', *IEEE Trans. Signal Process.*, 1994, **42**, (6), pp. 1376–1387
4 LI, F., and VACCARO, R.: 'Sensitivity analysis of DOA estimation algorithms to sensor errors', *IEEE Trans. Aerosp. Electr. Syst.*, 1992, **28**, pp. 708–717
5 VIBERG, M., and SWINDLEHURST, A.L.: 'Analysis of the combined effects of finite samples and model errors on array processing performance', *IEEE Trans. Signal Process.*, 1994, **42**, pp. 3073–3083
6 STOICA, P., and NEHORAI, A.: 'MUSIC, maximum likelihood, and Cramér-Rao lower bound: Further results and comparisons', *IEEE Trans. Acoust. Speech Signal Process.*, 1990, **ASSP–37**, pp. 2140–2150
7 STOICA, P., and NEHORAI, A.: 'Performance comparison of subspace rotation and MUSIC methods for direction finding', *IEEE Trans. Signal Process.*, 1991, **39**, pp. 446–453
8 VIBERG, M., and OTTERSTEN, B.: 'Sensor array processing based on subspace fitting', *IEEE Trans. Signal Process.*, 1991, **39**, pp. 1110–1121
9 SWINDLEHURST, A., and KAILATH, T.: 'A performance analysis of subspace-based methods in the presence of model errors: Part I – the MUSIC algorithm', *IEEE Trans. Signal Process.*, 1992, **40**, pp. 1758–1774
10 SWINDLEHURST, A., and KAILATH, T.: 'A performance analysis of subspace-based methods in the presence of model errors: Part II – multidimensional algorithms', *IEEE Trans. Signal Process.*, 1993, **41**, pp. 2882–2890
11 XU, X.-L., and BUCKLEY, K.M.: 'Bias analysis of the MUSIC location estimator', *IEEE Trans. Signal Process.*, 1992, **40**, pp. 2559–2569
12 HAMZA, R., and BUCKLEY, K.: 'An analysis of weighted eigenspace methods in the presence of sensor errors', *IEEE Trans. Signal Process.*, 1995, **43**, pp. 1140–1150
13 XU, X.-L., and KAVEH, M.: 'Theoretical comparisons for MUSIC-like DOA estimators'. Proceedings of ICASSP95, Detroit, USA, May 1995, pp. 1140–1150

14 KANGAS, A., STOICA, P., and SÖDERSTRÖM, T.: 'Finite sample and modelling error effects on ESPRIT and MUSIC direction estimators', *IEE Proc., Radar Sonar Navig.*, 1994, **141**, pp. 249–255
15 KANGAS, A., STOICA, P., and SÖDERSTRÖM, T.: 'Large-sample analysis of MUSIC and Min-Norm direction estimators in the presence of model errors', *Circuits Syst. Signal Process.*, 1995, **14**,
16 MOSES, R.L., SÖDERSTRÖM, T., and SORELIUS, J.: 'Effects of multipath-induced angular spread on direction of arrival estimators in array signal processing'. Proceedings of the IEEE/IEE workshop on *Signal processing methods in multipath environments*, Glasgow, Scotland, 20–21 April 1995, pp. 6–15
17 STOICA, P., and MOSES, R.: 'Introduction to spectral analysis' (Prentice Hall, Upper Saddle River, NJ, USA, 1997)
18 COMPTON, R.T. Jr.: 'Adaptive antennas – concepts and performance' (Englewood Cliffs, NJ, Prentice-Hall, 1988)
19 STEWART, G.W.: 'Introduction to matrix computations' (Academic Press, New York, 1973)
20 KRIM, H., FORSTER, P., and PROAKIS, J.G.: 'Operator approach to performance analysis of Root-MUSIC and Root-Min-Norm direction estimators', *IEEE Trans. Signal Process.*, 1992, **40**, pp. 1687–1696
21 STOICA, P., and SÖDERSTRÖM, T.: 'Statistical analysis of MUSIC and subspace rotation estimates of sinusoidal frequencies', *IEEE Trans. Signal Process.*, 1991, **39**, pp. 1836–1847
22 ROY, R., and KAILATH, T.: 'ESPRIT – estimation of signal parameters via rotational invariance techniques', *IEEE Trans. Signal Process.*, 1989, **ASSP–37**, (7), pp. 984–995
23 GIERULL, C.H.: 'Statistical analysis of the eigenvector projection method for adaptive spatial filtering of interference', *IEE Proc. Radar Sonar Navig.*, 1997, **144**, pp. 57–63
24 STOICA, P., and NEHORAI, A.: 'MUSIC, maximum likelihood, and Cramér-Rao bound', *IEEE Trans. Acoust. Speech Signal Process.*, 1989, **37**, pp. 720–741